Figure

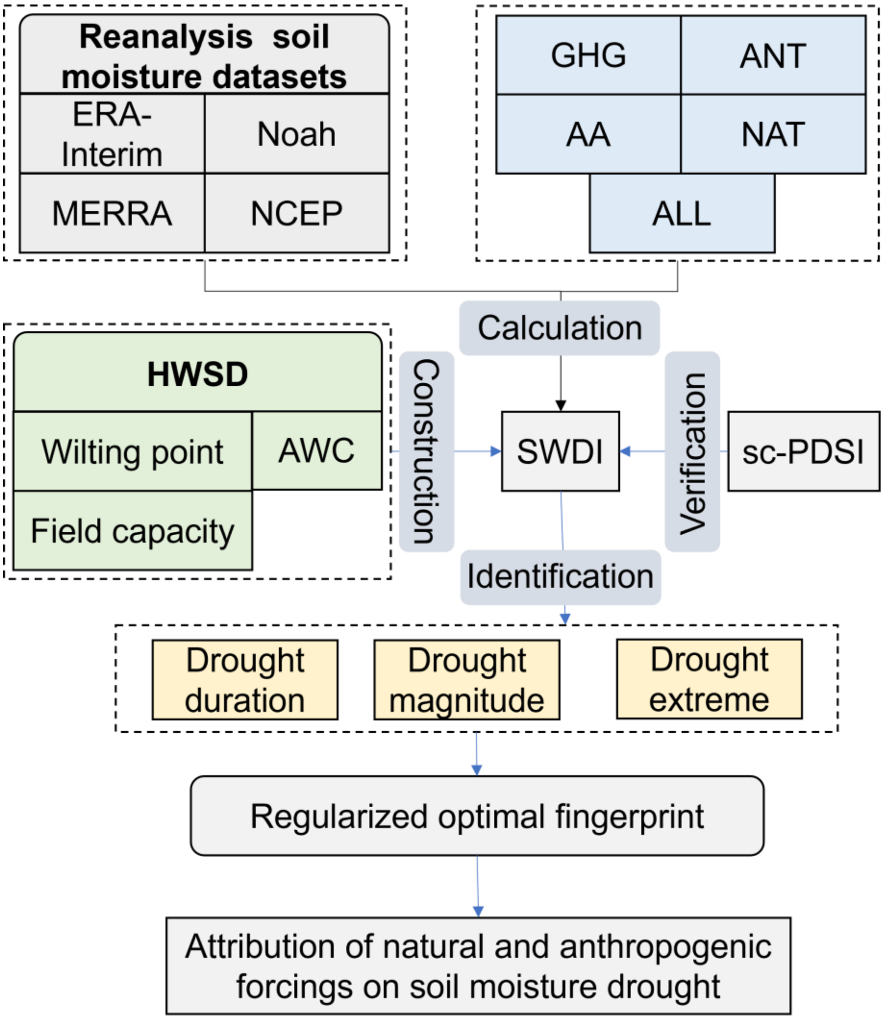

Figure 1. the flowchart of this study

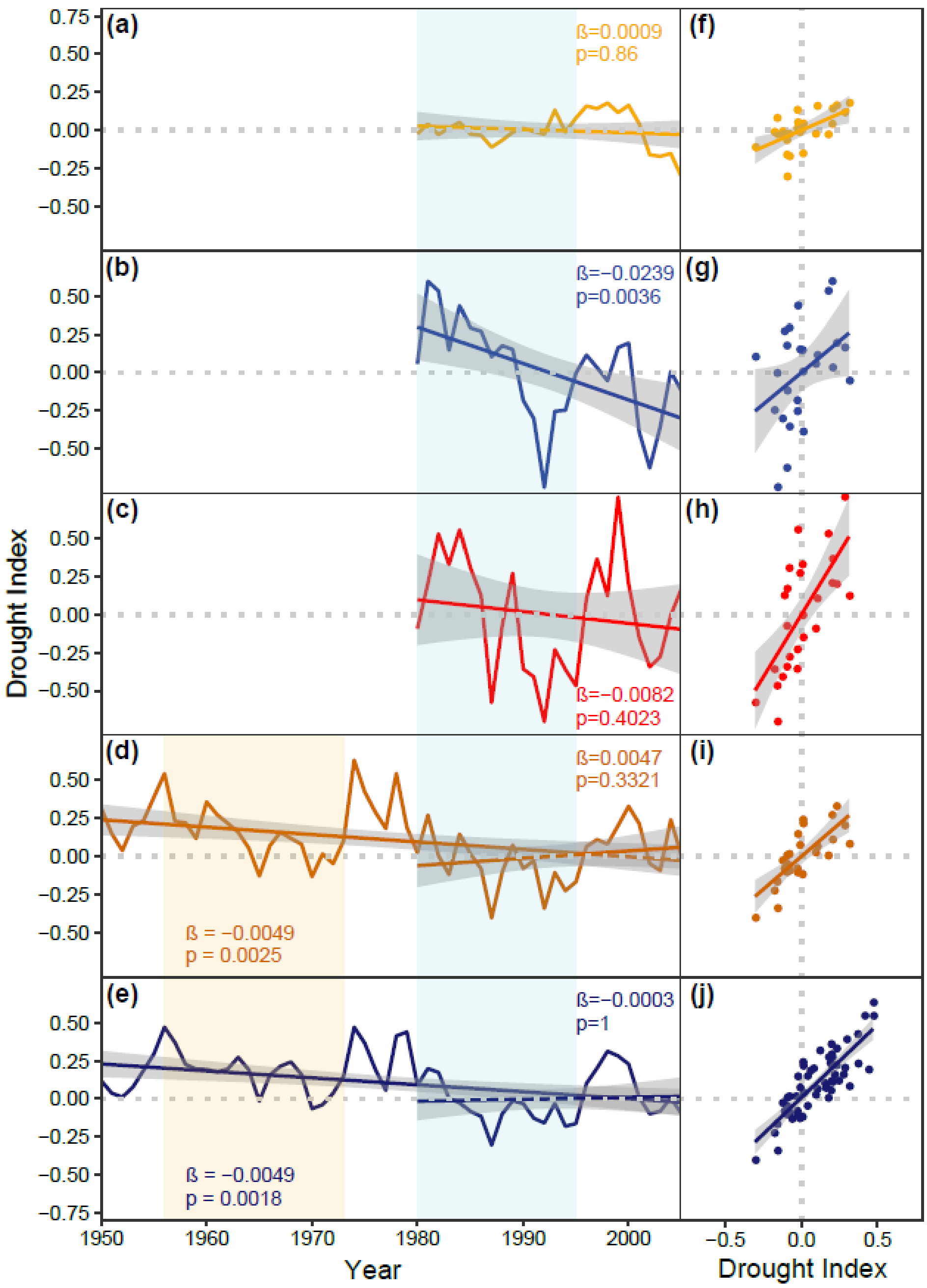

Figure 2. The time series of annual drought indices: SWDI derived from (a) ERA-Interim, (b) MERRA, (c) NCEP, (d) Noah soil moisture and (e) scPDSI. The slope (β) and p-value were denoted by Sen's slope method. The slope and p-value of two time periods of 1950-2005 and 1980-2005 were calculated for SWDI from Noah dataset and scPDSI. The scatter diagram of scPDSI with SWDI derived from (f) ERA-Interim, (g) MERRA, (h) NCEP, (i) Noah datasets during 1980-2005 and (j) scPDSI with SWDI derived from the Noah dataset during 1950-2005.

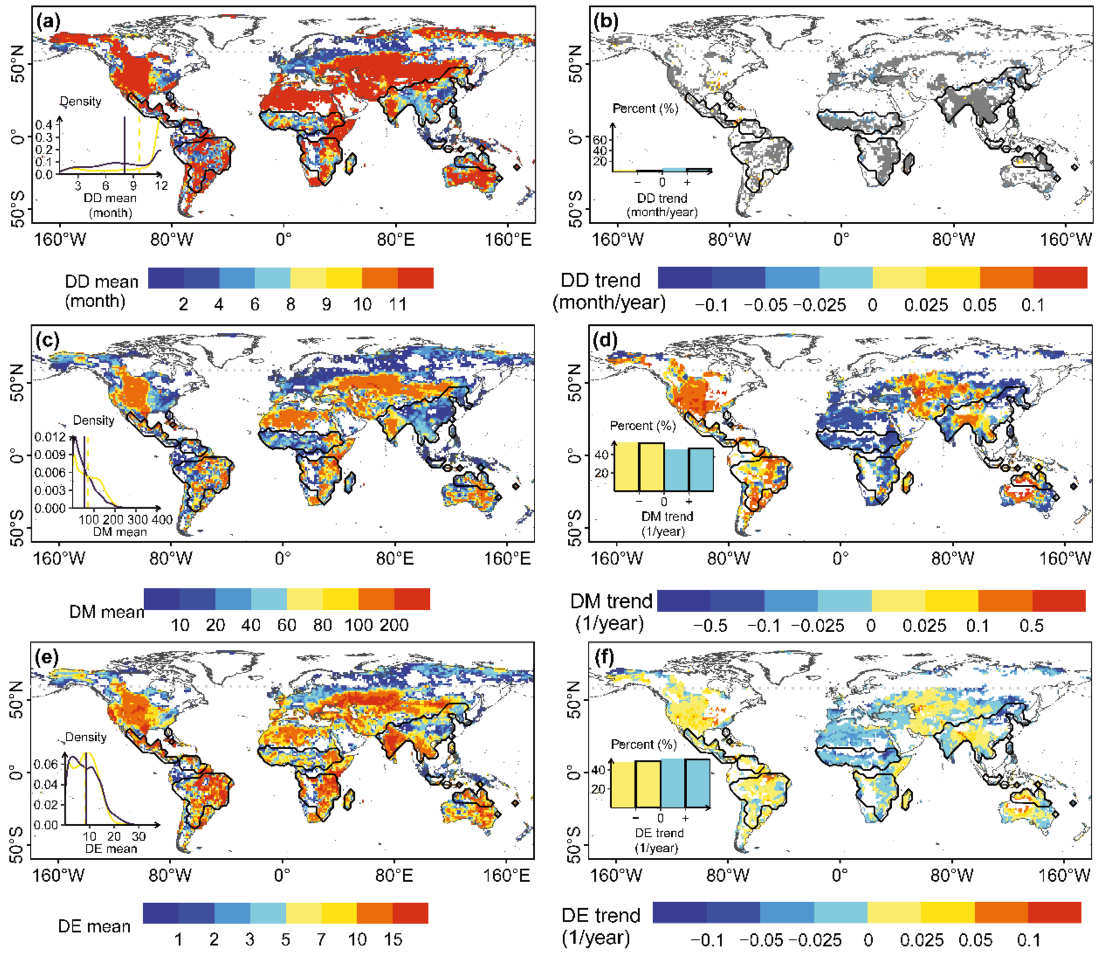

Figure 3. Global patterns and trends of annual (a) drought duration (DD), (b) drought magnitude (DM) and (c) drought extremum (DE) based on Noah soil moisture dataset during 1980-2005. The blue solid lines in the subgraph of the left panel also refer to the monsoon area, and the other line refers to the non-monsoon area. The bars with black solid rectangle line in the right panel refer to the monsoon area and the other bars refer to non-monsoon area. The gray color refers to where the trend is less than 10^{-3} month/year in the drought duration trend. The gray dotted line refers to the 60 ºN latitude.

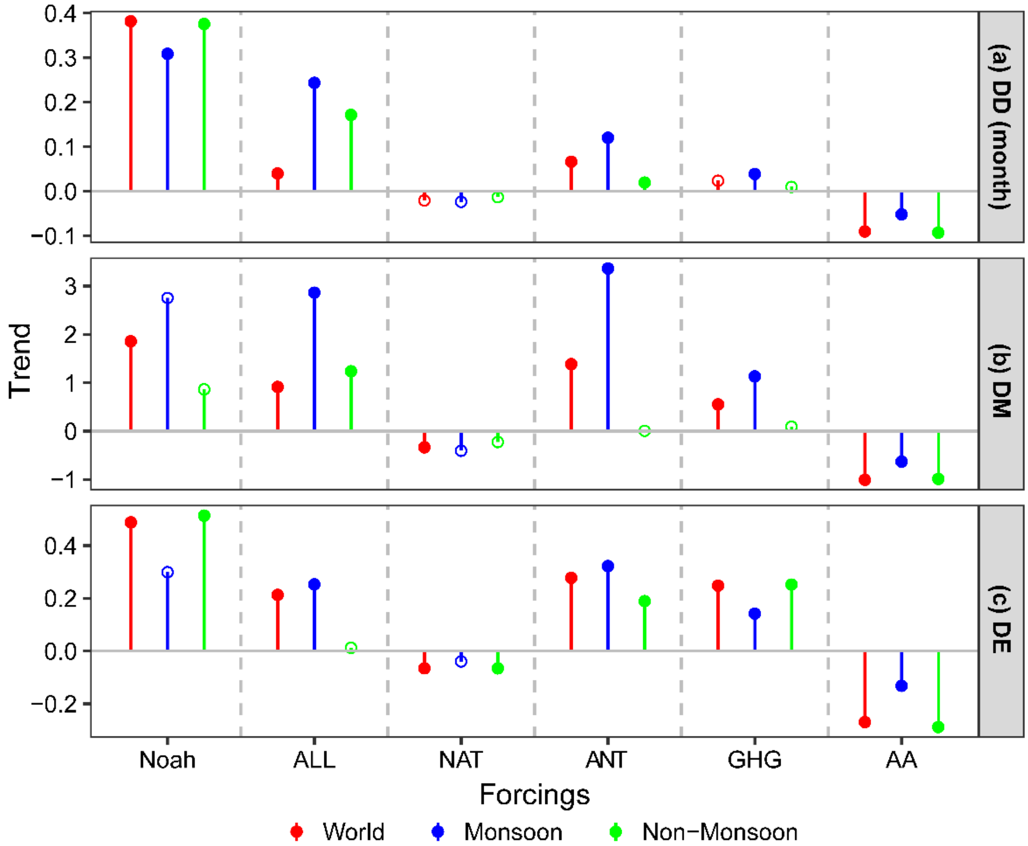

Figure 4. The trend of annual drought durations (DD), drought magnitude (DM), and drought extremum (DE) during 1951-2005 based on SWDI from the Noah soil moisture and different forcings in CMIP5. The colors refer to the different study areas: whole the world, the monsoon regions, and the non-monsoon regions. The solid colored points denote that the trends reach the significance level of 0.05, and the hollow dots conversely.

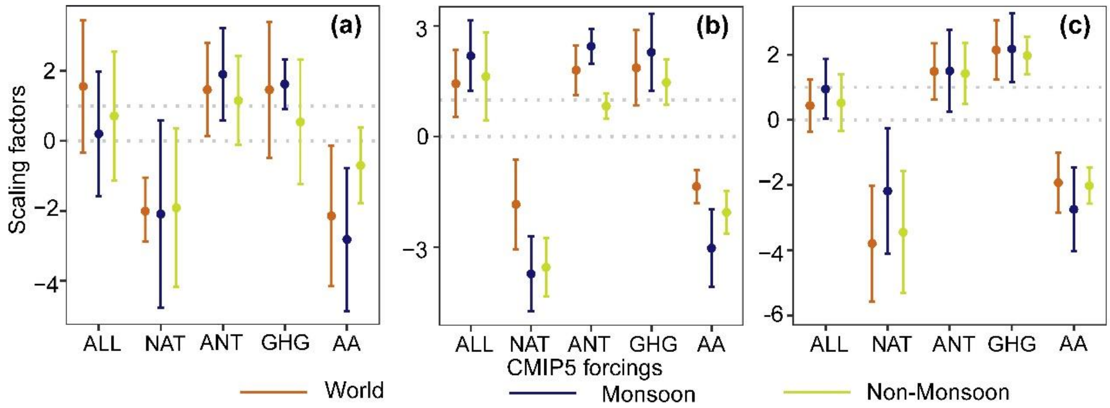

Figure 5. The scaling factor of annual (a) drought duration (DD), (b) drought magnitude (DM), and (c) drought extremum (DE) from a single-signal optimal fingerprint analysis. Different colors refer to three research areas: the whole world, monsoon regions and non-monsoon regions. The error bars indicate the 95% confidence intervals.

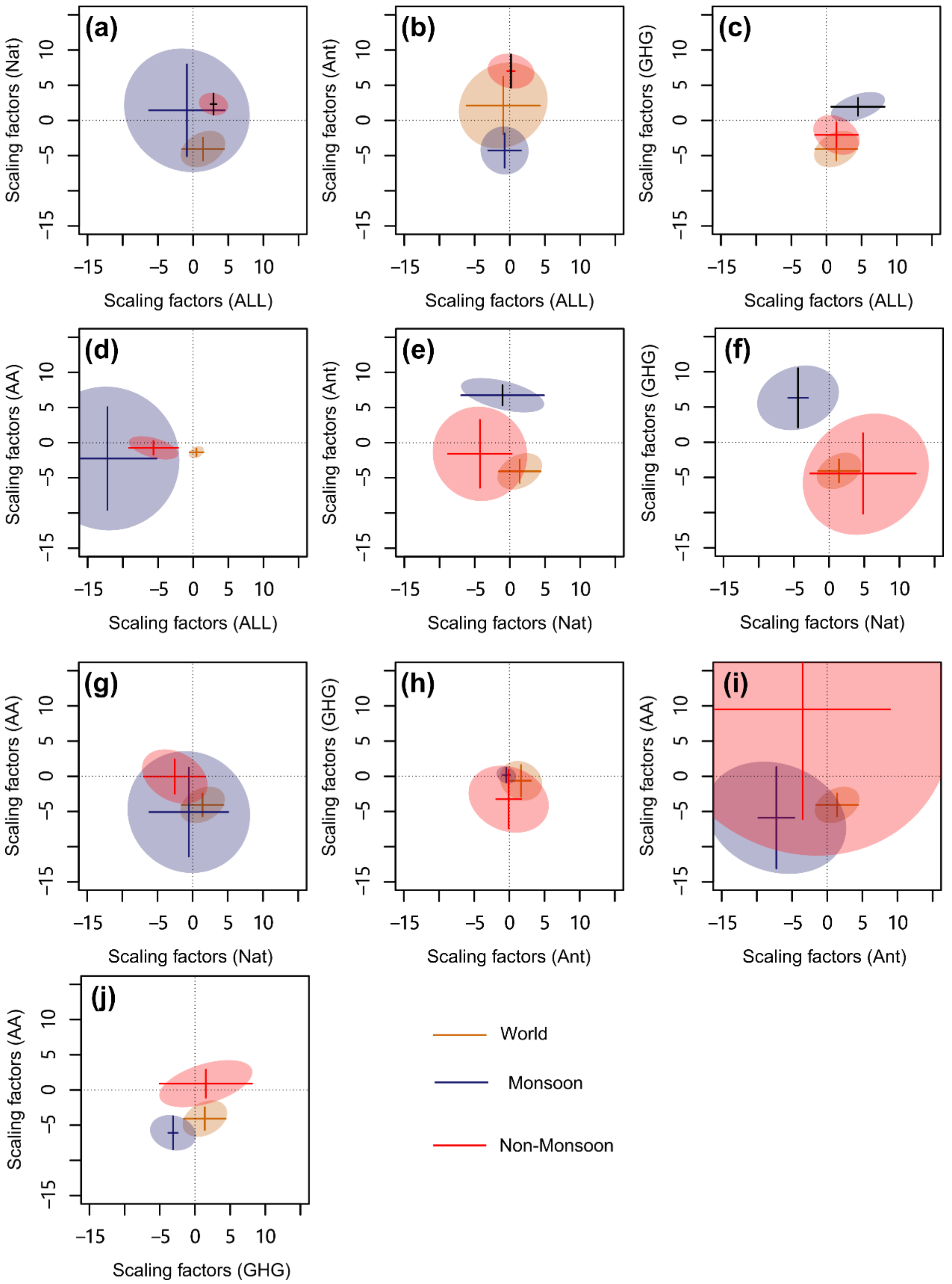

Figure 6. The scaling factor of annual drought duration (DD) from two-signal optimal fingerprint analysis and the shadows indicate the joint 95% confidence intervals. Different colors refer to three research areas: the whole world, monsoon regions and non-monsoon regions. Different dimensions refer to the corresponding forcings.

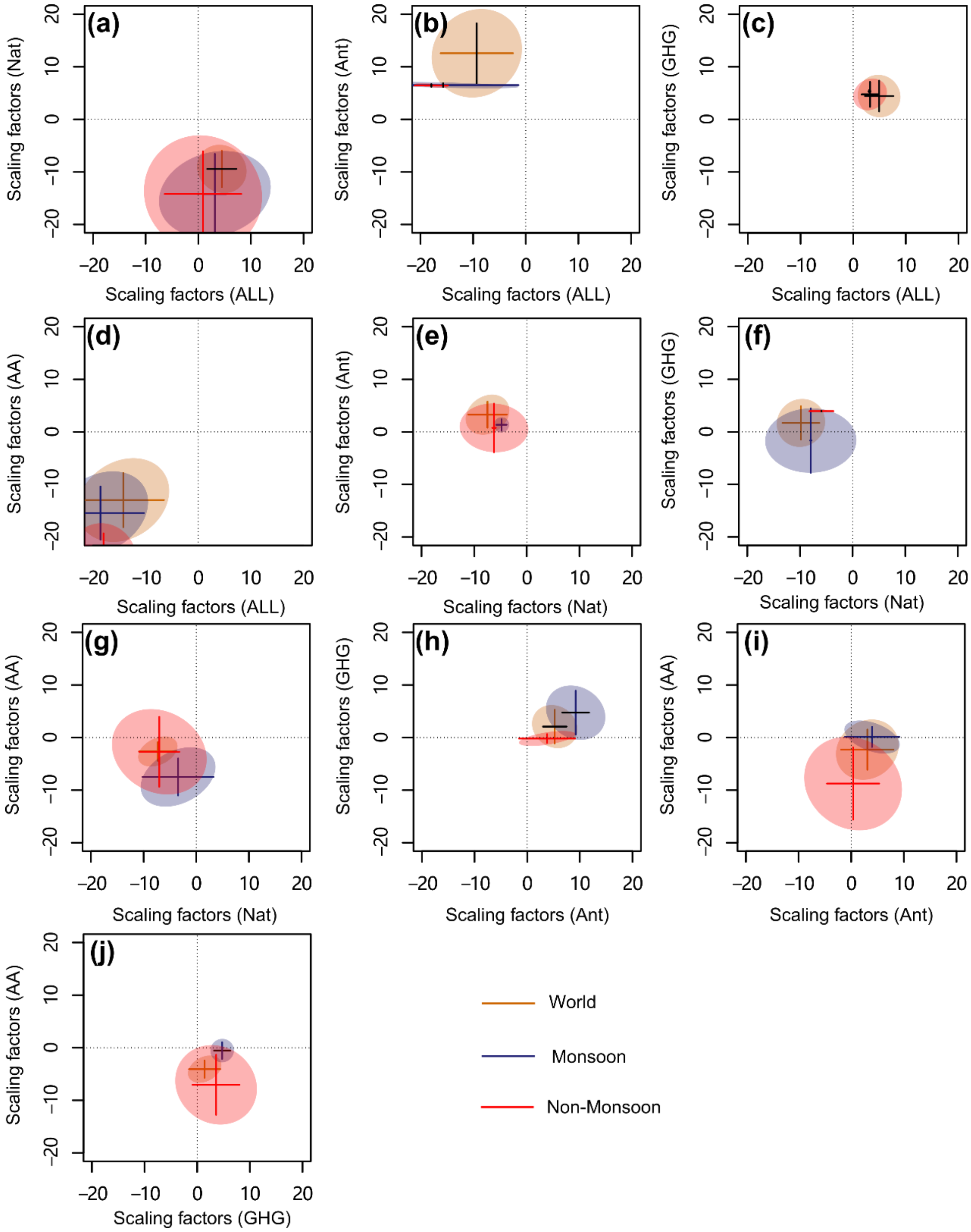

Figure 7. The scaling factor of annual drought magnitude (DM) from two-signal optimal fingerprint analysis and the shadows indicate the joint 95% confidence intervals. Different colors infer three research areas: the whole world, monsoon regions, and non-monsoon regions. Different dimensions refer to the corresponding forcings.

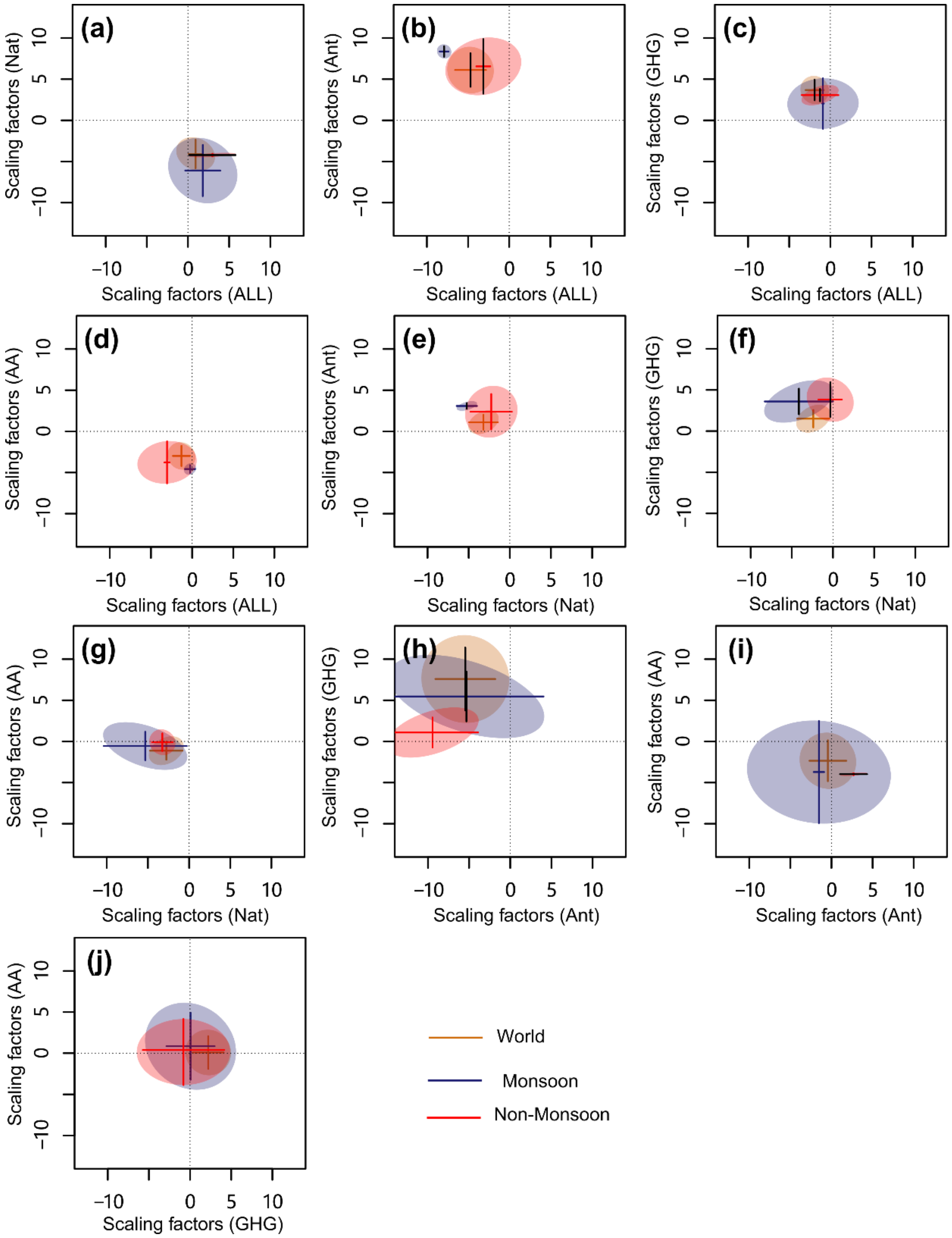

Figure 8. The scaling factor of annual drought extremum (DE) from two-signal optimal fingerprint analysis and the shadows indicate the joint 95% confidence intervals. Different colors refer to three research areas: the whole world, monsoon regions, and non-monsoon regions. Different dimensions refer to the corresponding forcings.

Global soil moisture drought identification and responses to natural and anthropogenic forcings

Keke Fan[1,2,3], Qiang Zhang[1,2,3], Xihui Gu[4], Vijay P. Singh[5], Chong-Yu Xu[6], Zexi Shen[1,2,3], Gang Wang[1,2,3]

1. Key Laboratory of Environmental Change and Natural Disaster, Ministry of Education, Beijing Normal University, Beijing 100875, China.

2. Faculty of Geographical Science, Academy of Disaster Reduction and Emergency Management, Beijing Normal University, Beijing 100875, China.

3. State Key Laboratory of Earth Surface Processes and Resource Ecology, Beijing Normal University, Beijing 100875, China.

4. Department of Atmospheric Science, School of Environmental Studies, China University of Geosciences, Wuhan 430074, China.

5. Department of Biological and Agricultural Engineering and Zachry Department of Civil & Environmental Engineering, Texas A&M University, College Station, Texas, USA. National Water and Energy Center, UAE University, Al Ain, UAE.

6. Department of Geosciences, University of Oslo, Postboks 1047, Blindern, 0316 OSLO, Norway.

Correspondence to: Qiang Zhang (zhangq68@bnu.edu.cn)

Abstract: The spatio-temporal patterns of drought changes and relevant forcings are still open for debate, especially under global warming, even though agricultural drought has long been receiving increasing concern for food security and sustainable development. In this study, we depicted global spatiotemporal patterns of agricultural drought using the Soil Water Deficit Index (SWDI) and reflected on the underlying forcings using the optimal fingerprint method. Three aspects of droughts were analyzed, i.e. drought duration (DD), drought magnitude (DM) and drought extremum (DE) over three regions, i.e. global, monsoon and non-monsoon regions. We found distinct spatial heterogeneity of DD, DM and DE. However, DM (DE) had mainly a decreasing (increasing) tendency. Anthropogenic activities (anthropogenic forcing only: including greenhouse gas, anthropogenic aerosol, and ozone [ANT]) and greenhouse gas changes (greenhouse gas forcing only [GHG]) played a prominent role in driving drought changes and were followed by the combination of anthropogenic and natural forcing (ALL). Soil moisture drought (DD, DM and DE) responses to external forcing of ANT and GHG were detected more easily in the monsoon region than in the non-monsoon region. Specifically, DM changes due to ANT (2.58 per century) contributed 39.88% of the DM changes by ALL (6.47 per century) in the monsoon regions, comparatively, the GHG and ANT induced changes of DM in the non-monsoon regions were quite slight. This study further clarified the impacts of anthropogenic warming on agricultural drought over the globe.

Key words: Soil moisture; SWDI; Forcings; Anthropogenic forcing; Attribution

analysis

1. Introduction

Drought, as an event of prolonged water deficit, is believed to be the costliest and least understood natural hazards with disastrous effects on agriculture, water supply, and economy (Mishra and Singh, 2010; Leng and Hall, 2019; Zhang et al., 2019a). Soil moisture (SM) is a pivotal linkage between land surface and atmosphere with respect to hydrothermal exchange (Zeng et al., 2015; Zhang et al., 2018a) and plays a critical role in the hydrological cycle (Zhang et al., 2018a). SM is also closely related to agricultural drought which is mainly characterized by SM deficit. Agricultural drought directly threatens food security and accentuates poverty (Pradhan et al., 2017; Yu et al., 2019) and has therefore been receiving increasing attention (e.g. Zhang et al., 2018b; Yu et al., 2019; Gu et al., 2019b). On the other hand, due to climate change (Dai, 2013) based on the evidence from model-simulated SM regimes (Wang, 2005; Gu et al., 2019b), drought indices (Yu et al., 2019), and precipitation-minus-evaporation (Seager et al., 2007), drought risk is expected to increase in the decades ahead. The Fifth Assessment Report of the Intergovernmental Panel on Climate Change pointed out low confidence since the middle of the 20th century in detecting the human impact on drought changes over global land areas due to internal climate variability (Yuan et al., 2019). Data scarcity and drought index variety (Sheffield et al., 2012; Yu et al., 2019) potentially produce large uncertainty in future drought projection (Samaniego et al., 2018; Yuan et al., 2019), and understanding the spatiotemporal patterns of SM drought

(SD) and relevant forcings are still a challenge in the backdrop of global warming (Gu et al., 2019b).

There is now sufficient evidence that global warming is intensifying the hydrological cycle at regional and global scales (Zhang et al., 2013; Mitchell et al., 2016; Ingram, 2016) and is therefore modifying water balances in both space and time, leading to the spatio-temporal redistribution of water resources and potentially threatening water resources security (Prudhomme et al., 2014). If global warming continues at the current rate, the difference between water supply and water demand will increase fivefold, and the current once-in-a-century drought will occur every 2 to 5 years in many regions (Naumann et al., 2018). Meanwhile, global monsoon precipitation provides the majority of water to agriculture and ecosystems (Deng et al., 2018), which have also led to the difference in climate between monsoon regions and non-monsoon regions. The increase of monsoon precipitation in the northern hemisphere promotes the occurrence of drought in the mid-latitudes by the monsoon-desert-like mechanism (Deng et al., 2018). SM drives land-atmosphere interactions via partitioning of precipitation and radiation (Albergel et al., 2013; Wanders et al., 2014), alters the hydrological cycle (Wanders et al., 2014), hydro-climatic extreme events (Padron et al., 2019), and modifies vegetation species (Roux et al., 2013). SM drought or agricultural drought hinders vegetation growth and agricultural production, causing reduced crop yield and food shortage and hence regional and global food security (Wheeler and von Braun, 2013). Therefore, it is critical to properly monitor and evaluate agricultural drought, reflecting on the spatiotemporal patterns of SM and relevant forcings in the monsoon and non-monsoon regions (Ochsner et al., 2013).

Many factors drive droughts and previous studies mainly focused on the impact of climate factors on droughts (Dai, 2013; Trenberth et al., 2014; Zhang et al., 2019b). The differentiation between human activities and climate change is of significance in the understanding of drought changes in both space and time and the mitigation of droughts, but limited attention has been paid in this aspect, especially at the global scale. Gu et al. (2019b) attributed SM drying to anthropogenic forcing at the global scale. Diffenbaugh et al. (2015) advocated that anthropogenic warming was increasing the likelihood of simultaneous warm and dry conditions in California. Based on hydrological and land-surface models, Samaniego et al. (2018) stated that anthropogenic warming exacerbated SD in Europe and new challenges for adaptation would have to be faced throughout the continent.

Currently, the research on exploring the effects of anthropogenic activities on drought is limited. First, the results based on different drought indices are quite different, and it is urgent to construct a reliable indicator that can accurately reflect agricultural drought. It should be noted that drought is multiscalar and can be described by duration, intensity or severity, inter-arrival time, and areal extent (Zhang & Zhou, 2015). The current research hardly focuses on the effect of different forcings on multiscalar characteristics of drought (including drought duration, drought degree, and extreme drought value). Moreover, these studies mainly focus on a single region, such as the whole world, and there is a lack of comparative studies in different regions. The monsoon region is greatly affected by the monsoon system, and monsoon precipitation provides most of the water sources for agriculture and ecosystems (Deng et al., 2018). The increase in monsoon precipitation promotes the occurrence of drought in the mid-latitude region through a monsoon-desert mechanism (Deng et al., 2018), which also leads to the difference in climate between monsoon and non-monsoon regions. In addition, there are still large differences in the intensity of anthropogenic activities in the monsoon and non-monsoon regions. It is therefore important to quantitatively analyze the impacts of different forcings (including natural forcing and anthropogenic forcing) on multiscalar characteristics of drought in the monsoon and non-monsoon regions. Therefore, the objectives of this study are: (1) to construct the Soil Water Deficit Index (SWDI) based on the Harmonized World Soil Dataset (HWSD) and the soil moisture reanalysis data that can best reflect the variation of drought; then depict the spatiotemporal patterns of multiscalar drought characteristics of drought duration (DD), drought magnitude (DM) and drought extreme (DE); and employ 282 ensembles from 31 CMIP5 models to explore the variation of DD, DM and DE under different historical forcing, including all forcing (ALL) , natural forcing (NAT), anthropogenic forcing (ANT), greenhouse gas forcing (GHG), and anthropogenic aerosol forcing (AA) in the global, monsoon and non-monsoon regions; further use the optimal fingerprint method to conduct the single and two-signal detection; finally identify and quantify the effects of different forcings on multiscale characteristics of drought.

2. Data

2.1 SM datasets

The Global Land Data Assimilation System (GLDAS) has been developed to optimally estimate land surface states and fluxes by ingesting satellite- and ground-based observed data products using advanced land surface models and data assimilation techniques (Rodell et al., 2004). GLDAS drives four models, including Noah, Mosaic, VIC and CLM, which are derived from the Goddard Earth Sciences Data and Information Services Center (http://disc.sci.gsfc.nasa.gov). The Noah model outputs global SM datasets of four layers (0~0.1 m, 0.2~0.4 m, 0.4~1 m and 1~2 m). The Noah V2.0 data products have a spatial resolution of 0.25℃× 0.25℃ and the time interval of 1948-2010, which has been used in many SM-related researches (Gu et al., 2019a; Zhang et al., 2019b). Meanwhile, ERA-Interim, MERRA (the Modern-Era Retrospective Analysis for Research and Application, Version 2) and NCEP-CFSR (the National Centers for Environmental Prediction-Climate Forecast System Reanalysis) were also used for the estimation of SM (Table S1). We resampled these SM data into the spatial scale of 0.25°×0.25° by bilinear interpolation method, and the study time range was 1980-2005, but 1950-2005 for Noah. The 0~1 m depth SM data were used for drought analysis from weighted average according to the depth of the upper three soil layers, which has been referred to as the root depth (Parajka et al., 2009; Santos et al., 2014; Yuan and Quiring, 2017). Due to the complex mechanism of frozen soil in high latitude areas, the SM content is generally high with higher uncertainty. In this study, we analyzed the SD changes and relevant forcings over the monsoon and non-monsoon regions (Deng et al., 2018), respectively, and the study region was limited to 60° S - 60° N, and the global spatial patterns were displayed.

2.2 SM datasets from Coupled Model Intercomparison Project 5 (CMIP5)

The historical forcings considered in this study included anthropogenic and natural forcing (ALL), natural forcing (NAT), anthropogenic forcing (ANT, including greenhouse gas, anthropogenic aerosol, and ozone), greenhouse gas forcing (GHG) and anthropogenic aerosol forcing (AA; Gu et al., 2019b; Taylor et al., 2012). The monthly SM datasets (variable "mrlsl") at the depth closest to 100 cm from CMIP5 were analyzed (Gu et al., 2019b), and the SM datasets from 31 models were used for ongoing analysis (Table S3). The SM datasets under different forcings are displayed in Tables S4-S8. 100 realizations of models and corresponding ensembles were used for the ALL forcing (Table S4), accordingly, 68 realizations for the NAT forcing (Table S5), 64 realizations for the GHG forcing (Table S6), 22 realizations for the AA forcing (Table S7), and 28 realizations for the ANT forcing (Table S8).

2.3 Harmonized World Soil Database (HWSD)

The Harmonized World Soil Database v 1.2 was released in 2012 jointly by Food and Agriculture Organization of the United Nations (FAO) with International Institute for Applied Systems Analysis (IIASA), the International Soil Reference and Information Centre (ISRIC-World Soil Information), Institute of Soil Science - Chinese Academy of Science (ISSCAS) and the Joint Research Centre of the European Commission (JRC). It is a 30-arc-second raster database that contains more than 15000 different soil mapping units and existing regional and national updates of soil information worldwide, combining the 1:5000000 scale FAO-UNESCO (United Nations Educational, Scientific, and Cultural Organization) Soil Map of World (FAO, 1971-1981). Although several new soil property datasets have been developed, HWSD V1.2 still have been widely used by researchers and are well validated and tested. The soil characteristics from HWSD are reliable for the research related to carbon capture, land use change, soil loss estimation, soil organic carbon stock, hydrological modelling, ecosystem services and so on (Ding et al., 2020; Nachtergaele et al., 2012; Othman et al., 2021; Rivas-Tabares et al., 2020; Shepherd et al., 2021; Suroso et al., 2021; Silatsa et al., 2020; Wenjie et al., 2020). (Nachtergaele et al., 2012). Sand, clay, and organic carbon were used to calculate field capacity and wilting point by the weighted average of top layer (0-30 cm) and sublayer (30-100 cm).

2.4 Self-calibrated Palmer Drought Severity Index (scPDSI)

We monitored and verified droughts using the scPDSI (Self-calibrated Palmer Drought Severity Index; Wells et al., 2004) from CRU TS 4.03 (Climatic Research Unit gridded Time Series Version 4.03), which is derived from monthly climate anomalies based on the fourth release of the new interpolation algorithm and can be applied in agricultural drought monitoring (Harris et al., 2020). PDSI was one of the first procedures to quantify drought severity under different climatic conditions (Palmer, 1965). Palmer's goal was to develop a general method for assessing drought based on an index capable of temporal and spatial comparisons of drought (Palmer, 1965). PDSI is based on the primitive water balance model (Wells et al., 2004), including a twostage "bucket" model for soils. The top layer can hold an inch of moisture, while the amount of moisture the lower soil can hold is a location-dependent value that must be provided as an input parameter (Wells et al., 2004).

The self-calibration characteristics of scPDSI are developed for each site and vary according to the climatic conditions. These constants are dynamically calculated based on the characteristics of each site location. The scPDSI is calculated from many gridded variables, such as temperature, precipitation, vapor pressure, and 10 m wind speed. Otherwise, potential evapotranspiration is calculated by a more physics-based Penman-Monteith parameterization, using actual vegetation cover rather than reference crop. Meanwhile, seasonal snow dynamics is included in the embedded water balance model (Van der Schrier et al., 2013). The scPDSI data used in this study spans the period of 1901-2018 at monthly scale and covers the global land surface except Antarctica with a 0.5° latitude and 0.5° longitude grid (Van der Schrier et al., 2013; Blunden and Arndt, 2019).

3. Methods

3.1 Soil Water Deficit Index (SWDI)

SWDI was proposed to monitor the agriculture drought based on basic soil water parameters and root zone SM (Martinez-Fernandez et al., 2015). The satisfactory drought monitoring performance of SWDI has been well corroborated (Martinez-Fernandez et al., 2016; Zhu et al., 2019). SWDI was defined as:

$$\mathrm{SWDI} = \frac{\theta - \theta_{FC}}{\theta_{AWC}} \times 10 \quad (1)$$

$$\theta_{AWC} = \theta_{FC} - \theta_{WP} \quad (2)$$

where θ is the SM content in the root zone soil layer (m^3/m^3); θ_{FC} denotes the field capacity (FC), θ_{WP} represents the wilting point (WP), and θ_{AWC} denotes the available water content (AWC). The SWDI, multiplied by 10, is a range of values with agricultural implication in terms of available soil water (Martinez-Fernandez et al., 2015) to be classified into different drought levels (Table S2). Here we assumed that the SM content was favorable for crop growth given certain field capacity. The positive SWDI values indicated too much water in the soil. When it was close to zero, the soil water reached field capacity (i.e. no water excess and deficit); when SWDI was negative, the agriculture drought occurred and the impact of drought depended on the crop type and the proportion of available soil water that could be used from the root zone before water stress occurred (Allen et al., 1998; Martinez-Fernandez et al., 2015 and 2016).

3.2 Soil features

There are three main ways to define θ_{FC} and θ_{WP}: (1) the 5th and 95th percentiles of soil water contents represented by θ_{WP} and θ_{FC}; (2) soil water contents at the water potential of -1500 kPa and -33 kPa denoted as θ_{WP} and θ_{FC}; (3) θ_{WP} and θ_{FC} were obtained by basic physical characteristics of soil (i.e., the proportion of sand and clay, and the organic matter content) via pedo-transfer functions (Zhu et al., 2019; Parchami-Araghi et al., 2013). Zhu et al. (2019) chose the 5^{th} and 95^{th} percentiles of SM during the growing season as the annual θ_{WP} and θ_{FC}. Martinez-Fernandez et al. (2016) employed several methods to obtain θ_{WP} and θ_{FC} and found that the temporal variation and the range of the index derived by the first method were unrealistic. Results by the second way identified the drought dynamics better than the other ways (Martinez-Fernandez et al., 2016). Generally, the soil water contents at the water potential of -1500 kPa and -33 kPa were accepted as θ_{WP} and θ_{FC} (Parchami-Araghi et al., 2013; Martinez-Fernandez et al., 2015, 2016) and were computed as:

$$\theta_{1500} = \theta_{1500f} + \left(0.14 \times \theta_{1500f} - 0.02\right) \tag{3}$$

where $\theta_{1500f} = -0.024S + 0.487C + 0.006OM + 0.005(S \times OM) - 0.013(C \times OM) + 0.068(S \times C) + 0.031$

$$\theta_{33} = \theta_{33t} + \left[1.283\left(\theta_{33f}\right)^2 - 0.374\left(\theta_{33f}\right) - 0.015\right] \tag{4}$$

where $\theta_{33f} = -0.251S + 0.195C + 0.011OM + 0.006(S \times OM) - 0.027(C \times OM) + 0.452(S \times C) + 0.299$

where θ_{1500} denotes the -1500 kPa SM, i.e. θ_{WP}. θ_{1500f} denotes the -1500 kPa SM of the first solution. Similarly, θ_{33} denotes the -33 kPa SM, i.e. θ_{FC}. θ_{33f} denotes the -33 kPa SM of the first solution. S, C, and OM refer to the proportion of sand, the proportion of clay and the organic matter content, respectively. In general, the organic matter content was derived from the organic carbon (OC) divided by the van Bemmelen factor of 0.58 (Minasny & Mcbratney, 2018). OM was calculated as:

$$OM = 1.724 \times OC \tag{5}$$

where OC denotes the organic carbon content. S, C and OC were obtained from the HWSD.

3.3 Verification of SWDI

SWDI was calculated based on four different monthly SM datasets: ERA-Interim, MERRA, NCEP, and Noah, respectively. Whether or not they could characterize the agriculture drought worldwide needed to be further evidenced. Here we chose the scPDSI as a reference drought index (Barichivich et al., 2019), and we evidenced drought monitoring performance of SWDI based on these four SM datasets against the scPDSI from a spatiotemporal viewpoint.

3.4 Definition of drought

Clarification of the definition of drought is the first step into drought risk evaluation. Drought was considered to occur when SWDI was less than or equal to 0. Drought duration (DD) was defined as the number of months when drought occurred within one year; drought magnitude (DM) was defined as the accumulation of the absolute value of SWDI during the occurrence of drought within one year; drought extremum (DE) was defined as the maximum of the absolute value of SWDI during the occurrence of drought within one year. Meanwhile, the grids with positive SWDI were removed from the analysis in that SWDI>0 meant no drought.

3.5 Regularized optimal fingerprinting method (ROF)

The optimal fingerprinting technique has been widely used for analyzing the detection and attribution of climate change (Zhang et al., 2007; Ribes et al., 2009). The regularized optimal fingerprinting method (ROF) was proposed by Ribes et al. (2013) and has been widely used for quantifying the anthropogenic contribution to climate and hydrological changes (Zhang et al., 2007; Gudmundsson et al., 2017; Slangen et al., 2014; Ribes & Terray, 2013; Gu et al., 2019b). Assuming a noiseless model-based response mode, the standard detection model is as follows (Allen & Tett, 1999; Hannart, 2016; Gu et al., 2019b):

$$\mathrm{Y} = \sum_{i=1}^{m} x_i \beta_i + \varepsilon = X\beta + \varepsilon$$

Where Y is the rank-n vector of observed values, X is the climate model-simulated values, m is the number of climate fingerprint parrerns, and ε is the internal uncertainty of Y. The total least squares approach was used to estimate the scale factor ε which adjusts the magnitude of the fingerprint regression to best match observations. The estimates of the scale factor (β) and corresponding confidence intervals rely on covariance matrices representing internal climate variability (i.e., climate "noise") and are estimated from independent subsamples in pre-industrial conditions (Gudmundsson et al., 2017; Slangen et al., 2014; Ribes & Terray, 2013; Gu et al., 2019b).

4. Results

4.1 Verification of SWDI

Soil water characteristics can be used to further improve the performance of SWDI (Fig. S1). The global average of the AWC in this study was 0.109 m^3/m^3. Moreover, the spatial patterns of the estimated SM based on four SM datasets captured dry and wet conditions of the root zone SM across the globe (Fig. S2), indicating that the global mean SM was about 0.25 m^3/m^3. Reliable soil water characteristics and high-quality

SM datasets combined to result in the accurate evaluation of SWDI and were used to evaluate the drought conditions at the global scale (Dorigo et al., 2015).

We found drought-affected areas of severe drought > moderate drought > extreme drought > mild drought, despite different spatial patterns of SWDI based on four datasets (Fig. S3). Drought monitoring results by SWDI indicated a drying tendency in the non-monsoon region except for the high-altitude area. The SWDI based on different datasets also showed consistent spatial patterns of droughts, such as severe droughts monitored in South America, Africa, and Central Asia (Sheffield et al., 2014), wherein the results by SWDI based on the Noah indicated that droughts occurred across 73.62% of the continents over the world. Meanwhile, the SWDI based on the Noah identified the droughts in northern North America, northeastern Russia, and Australia (Naumann et al., 2018) as those monitored by scPDSI (Fig. S4). From the spatial patterns of annual mean and trends of scPDSI (Fig. S4), we observed similar changing patterns of drying and/or wetting tendency within the monsoon region when compared with the non-monsoon region, while the drying tendency dominated in the monsoon region (58.32%). The regions close to the ocean were characterized by the wetting tendency and the regions with the drying tendency were far away from the sea in the monsoon region (Dai, 2013).

The annual changes of drought indices, such as SWDI based on four SM datasets and scPDSI, were displayed in Fig. 2. scPDSI and SWDI based on the Noah SM dataset were decreasing during 1950-2005, indicating intensifying droughts with Sen's Slope value of -0.49 every century ($P < 0.05$, Figs. 2d-e). Besides, persistently intensifying droughts were observed during two periods of 1956-1970 and 1980-1995 (Figs. 2b-e). Droughts by scPDSI during 1980-2005 did not significantly change (Van der Schrier et al., 2013). The SWDI based on the MERRA SM dataset indicated enhanced droughts with a rate of about -0.02 every year ($P < 0.05$). Droughts by the SWDI based on the Noah SM dataset were subject to similar variations when compared to the droughts by the scPDSI. Even droughts by the SWDI based on the NCEP SM data followed a similar variation but the amplitude of drought was more severe than by the Noah-based SWDI and severe droughts occurred in 1987 (Figs. 2c-e). The period of 1990-1995 witnessed long lasting droughts with the drought indices less than 0 (Figs. 2b-e). Furthermore, droughts were underestimated by SWDI based on the ERA-Interim SM data when compared to scPDSI (Fig. 2f). Comparatively, droughts were overestimated by the SWDI based on the NCEP SM data (Fig. 2h). Meanwhile, Fig. 2g indicated that the SWDI based on the MERRA SM data did not capture the droughts well when compared to scPDSI. The SWDI values from Noah SM during 1980-2005 and 1950-2005 were in good relationship with scPDSI with the scatter points around the straight line (Figs. 2i and j). In general, results showed that SWDI values based on four SM datasets were in positive correlation with scPDSI within most areas (about 90% of the study region). The SWDI values based on ERA-Interim and MERRA had similar drought monitoring performance with more than half areas being evaluated well which was inferior to that from Noah (Fig. S5; Li et al., 2020).

4.2 Drought changes evaluated based on Noah SM dataset

Fig. 3 demonstrates the spatial patterns and trends of historical drought conditions, including annual DD, DM and DE based on the Noah SM dataset. The DD in the non-monsoon region was obviously longer than that in the monsoon region. Most areas of the non-monsoon region were dominated by the duration of more than 9 months, comparatively, the DD in the monsoon region was in the range of 0-12 months. Sheffield et al. (2012) considered the changes in the available energy, humidity and wind speed and found little changes in drought during the past 60 years. Most grids were dominated by invariant DD (Fig. 3b). The S-shape drought density line for multi-year mean DM in the non-monsoon region indicated that a considerable number of grids were characterized by severe droughts. More grids displayed a decreasing trend of DM in both non-monsoon (50.13%) and monsoon (49.27%) regions, even though the grids for weakening and strengthening DM were near half of all the grids considered, wherein DM tended to increase in the monsoon region, such as Asia and South America, implying that these regions were dominated by intensifying droughts, while the African monsoon areas had a wetting tendency. DE Unlike DM, there were more areas with extreme DE in the monsoon region than in the non-monsoon region. Meanwhile, the DE had an increasing trend in both non-monsoon (48.72% of area) and monsoon (48.04% of area) regions, indicating that DE slightly increased, which was also different from DM. The spatial patterns of DE were similar to DM. Zhai et al. (2017) analyzed the intensity-area-duration of droughts and found significantly different trends among them which was consistent with the results in this study.

4.3 Drought changes under different forcings

The temporal variations of drought features based on the Noah SM dataset, such as DD, DM, and DE, during 1951-2005 under different history forcings are shown in Figs. 4 and S6-S8. The anomalies of DD had a significant increase by 0.4 month/century ($P < 0.05$) during 1951-2005, while these anomalies first increased during 1951-1991 and then decreased during 1992-2005, indicating the weakening drought condition in terms of duration (Fig. S6). No significant decrease was detected ($P > 0.05$) mainly under the NAT forcing even with decreasing DD (Fig. 4). Under the GHG forcing, only in the monsoon region, there was significant drying, which indicated that the increase of greenhouse gases induced by anthropogenic forcing significantly increased the DD in the monsoon region over the globe. Only under the AA forcing, the DD significantly decreased, indicating that aerosols greatly alleviated droughts by reflecting the downward short radiations and further retarding evapotranspiration (Mahowald, 2011; Liu et al., 2016).

The DM in the monsoon region had a more significant increase than in the non-monsoon region, especially under the ANT and GHG forcings. The ANT forcing caused an increasing trend in the DM by 3.36 per century, which was much greater than the increasing magnitude under the GHG forcing. Meanwhile, the DM decreased due to the AA forcing, indicating that anthropogenic forcing except GHG were potentially exacerbating the DM. The DM by SWDI based on the Noah SM dataset increased significantly by 1.86 per century over the globe and had insignificant trends over the monsoon and non-monsoon regions.

The DE by SWDI based on the Noah SM data had an insignificant increase across the monsoon region. Different forcings had different effects on droughts over the monsoon and non-monsoon regions, respectively. Otherwise, the AA forcing had similar effects on droughts when compared to other forcings, such as ALL, ANT and GHG, indicating that AA had a profound driving effect on the DE relative to the duration and the intensity. The impacts of ALL on droughts were akin to ANT and even NAT alleviated droughts. The drought changes in the non-monsoon region due to the above-mentioned forcings told different stories, indicating that anthropogenic forcing in the non-monsoon region were not so intense when compared to those in the monsoon region, while natural forcing still had a certain effect on drought changes.

4.4 Results by single-signal optimal fingerprint method

Fig. 4 shows the scaling factors of annual DD, DM and DE by a single-signal optimal fingerprint analysis. The significance values of most forcings were not larger than zero, indicating that the effects of most forcings on DD were not detectable. Except for DD, the values of most scaling factors were much larger than 1, indicating that the drought conditions under all forcings by CMIP5 were underestimated (Fig. 4; Yuan & Quiring, 2017). In general, the effects of ALL, ANT and GHG on droughts were detected for DM and DE. This was consistent with the findings that the global drying was mainly attributed to anthropogenic forcing under global warming (Dai et al., 2004; Gu et al., 2019b). The attribution analysis by the single-signal optimal fingerprint method for the NAT and AA forcings failed with the scaling factors less than zero (Fig.

5) for not only DD but also for DM and DE, indicating that the signals of NAT and AA in the global drought were not detectable (Chen & Sun, 2017). However, the ANT and GHG forcings for drought were still detected in the monsoon region with scaling factors of 2.65 and 2.46 for DM. The scaling factors in the monsoon region were within wider confidence ranges, indicating that the forcings had more uncertain effects on droughts in the monsoon region than in the non-monsoon region.

The values of linear trends of the multi-model in different forcings multiplied by the calculated scaling factors were taken as the attribution of droughts to different forcings. Among these forcings, the ANT and GHG forcings have been investigated widely (Gu et al., 2019b). The ANT-induced change in DD was 0.12 months/century at the global scale, comparatively, the ANT-induced change in DD in the monsoon region was more intense, being 0.20 months/century, while the GHG-induced change in the DD was quite small and the linear trend was near zero. The ANT-induced change in the DM was 1.76 per century at the global scale, while the regional difference was quite remarkable, wherein the ANT-induced change of DM was 6.47 per century in the monsoon region and the GHG-induced change in DM was 2.58 per century which accounted for 39.88% of the ANT-induced changes of DM, comparatively, the GHG and ANT induced changes of DM in the non-monsoon region were quite slight. The ANT-induced change of DE was similar within these three regions, which was 0.32 per century over the globe, being 0.36 per century in the monsoon region, and 0.21 per century in the non-monsoon region. But the GHG-induced change of DE was greater in the non-monsoon region (0.53 per century) than in the monsoon region (0.34 per century).

4.5 Results by two-signal optimal fingerprint method

Different drought metrics were affected by multiple different climate forcings, but the results by the single-signal optimal fingerprint method were obtained by only one signal when the trend value was much greater than the noise (Chen & Sun, 2017; Gu et al., 2019b). Therefore, the two-signal optimal fingerprint detection analysis was done to further explore whether one signal was separated from the other forcings for three drought metrics considered in this study (Zhang et al., 2013; Gu et al., 2019b). Figs. 6-8 show detection results for pairwise groups of five different forcings. Each forcing of most pairwise groups was not detected from the other. Specifically, the detection results of different combinations in different regions were significantly different.

For DD (Fig. 6), the scaling factors of ANT and GHG were greater than zero in the pair with NAT (Figs. 6e and 6f), which indicated that the forcings of ANT and GHG were detected from the NAT forcing in the monsoon region. Figs. 6a, 6b and 6c show that the NAT and ANT forcings in the non-monsoon region were detected, and GHG in the monsoon region was detected relative to the All forcing, which indicated that even the anthropogenic forcing impacted the DD, but the greenhouse gas was more significant for the DD variations in the monsoon region. For DM (Fig. 7), it was interesting that the forcings of GHG and All were detected from each other (Fig. 7c) and ANT was detected from the ALL forcing (Fig. 7b) in all three regions. To some extent, these results imply that the DM induced from the anthropogenic forcing including the emission of GHG significantly impacted DM. Besides, the scaling factors of ANT with GHG over the globe and the monsoon region (Fig. 7h), and the scaling factor of GHG with AA in the monsoon region were larger than zero (Fig. 7j), which indicated that the impact of the anthropogenic forcing was detected, and the different components of anthropogenic forcing like GHG and AA had significantly different impacts on DM.

For drought maximum (Fig. 8), the impact of anthropogenic forcing on the DE was more significant than the DD and DM. Generally, the scaling factors of ANT and GHG relative to ALL and NAT were greater than zero with the values in the second quadrant, implying that ALL and NAT were detected from ANT and GHG (Figs. 8b, 8c, 8e and 8f; Gu et al., 2019b). Specifically, the ANT forcing was detected significantly with ALL in all three regions (Fig. 8b), while the GHG was not detected significantly with ALL in the monsoon region (Fig. 8c). Only ANT in the monsoon region was detected significantly from NAT (Fig. 8e). Besides, the scaling factors of GHG relative to ANT over the globe and monsoon region were greater than zero (Fig. 8h) which indicated that GHG can be detected from ANT forcing. The different detection results indicated that the complexity and uncertainty of drought mechanisms showed that GHG-induced warming caused land surface aridity, but some recent studies reported that increased CO_2 led to the reduction of evaporation and hence mitigation of drought (Dai et al., 2018).

5. Conclusions

This study developed a drought index based on SM and soil water characteristics from HWSD, and then we conducted attribution analysis of anthropogenic forcing and natural forcing using the optimal fingerprint method. We obtained the following conclusions:

(1) More grids were dominated by decreasing DM in both non-monsoon and monsoon regions, even though the grids for weakening and strengthening DM were nearly half of all grids. Meanwhile, DE had an increasing trend in both non-monsoon and monsoon regions which was also different from DM.

(2) The effects of ANT and GHG on drought can be detected easier in the monsoon region than in the non-monsoon region, and the scaling factors with greater confidence range indicated the effects varied greatly due to spatial heterogeneity in the monsoon region. The ANT-induced change of DM was 1.76 per century over the globe, but the regional difference was quite remarkable. Meanwhile, the ANT-induced change of DM was 6.47 per century in the monsoon region and the GHG-induced change of DM was 2.58 per century which accounted for 39.88% of the ANT-induced change of DM. The ANT-induced change of DE was similar in the three regions, which was 0.32 per century over the globe, being 0.36 per century in the monsoon region, and 0.21 per century in the non-monsoon region.

(3) The impact of anthropogenic forcing on DE was more significant relative to the DD and DM. For DD and DM, ANT and GHG were easily detected from ALL in the three regions and GHG also was detected from ANT in the monsoon region. But for DE, ANT and GHG were also detected from NAT.

Acknowledgments: This research has been financially supported by the China National Key R&D Program, Grant No. 2019YFA0606900, the National Science Foundation of China, Grant No. 41771536, and the National Science Foundation for Distinguished Young Scholars of China, Grant No. 51425903. All authors declare no conflict of interest. Here we are thankful to editor, Prof. Dr. Sally Elizabeth Thompson, and anonymous reviewers for their professional comments and suggestions which are greatly helpful for further quality improvement of this current manuscript.

References:

Albergel, C., Dorigo, W., Reichle, R.H., Balsamo, G., De Rosnay, P., Munoz-Sabater, J., Isaksen, L., De Jeu, R., Wagner, W., 2013. Skill and global trend analysis of soil moisture from reanalyses and microwave remote sensing. J. Hydrometeorol. 14(4), 1259-1277. https://doi.org/10.1175/JHM-D-12-0161.1.

Allen, R.G., Pereira, L.S., Raes, D., Smith, M., 1998. Crop evapotranspiration: Guidelines for computing crop water requirements, FAO irrigation and drainage paper 56. Rome: FAO. https://appgeodb.nancy.inra.fr/biljou/pdf.

Allen, M. R., & Tett, S. F. 1999. Checking for model consistency in optimal fingerprinting. Clim. Dyn. 15(6), 419-434. https://doi.org/10.1007/s003820050291

Blunden, J., Arndt, D.S., 2019. State of the Climate in 2018. Bull. Am. Meteorol. Soc. 100(9), Si-S306. https://doi.org/10.1175/2019BAMSStateoftheClimate.1.

Chen, H., Sun, J., 2017. Contribution of human influence to increased daily precipitation extremes over China. Geophys. Res. Lett. 44(5), 2436-2444. https://doi.org/10.1002/2016GL072439.

Dai, A., Trenberth, K.E., Qian, T., 2004. A global dataset of Palmer Drought Severity Index for 1870–2002: Relationship with soil moisture and effects of surface warming. J. Hydrometeorol. 5(6), 1117-1130. https://doi.org/10.1175/JHM-386.1.

Dai, A., 2013. Increasing drought under global warming in observations and models. Nat. Clim. Chang. 3(1), 52-58. https://doi.org/10.1038/NCLIMATE1633.

Dai, A., Zhao, T., Chen, J., 2018. Climate change and drought: A precipitation and evaporation perspective. Curr. Clim. Change. Rep. 4(3), 301-312. https://doi.org/10.1007/s40641-018-0101-6.

Deng, K., Yang, S., Ting, M., Tan, Y., He, S., 2018. Global monsoon precipitation: Trends, leading modes, and associated drought and heat wave in the Northern Hemisphere. J. Clim. 31(17), 6947-6966. https://doi.org/10.1175/JCLI-D-17-0569.1.

Diffenbaugh, N.S., Swain, D.L., Touma, D., 2015. Anthropogenic warming has increased drought risk in California. Proc. Natl. Acad. Sci. U. S. A. 112(13), 3931-3936. https://doi.org/10.1073/pnas.1422385112.

Ding, J., Yang, S., Shi, Q., Wei, Y., & Wang, F. (2020). Using Apparent Electrical Conductivity as Indicator for Investigating Potential Spatial Variation of Soil Salinity across Seven Oases along Tarim River in Southern Xinjiang, China. Remote Sensing, 12(16), 2601.

Dorigo, W.A., Gruber, A., De Jeu, R.A.M., Wagner, W., Stacke, T., Loew, A., Albergel, C., Brocca, L., Chung, D., Parinussa, R.M., Kidd, R., 2015. Evaluation of the ESA CCI soil moisture product using ground-based observations. Remote Sens. Environ. 162, 380-395. https://doi.org/10.1016/j.rse.2014.07.023.

Gu, X., Zhang, Q., Li, J., Singh, V.P., Liu, J., Sun, P., He, C., Wu, J., 2019a. Intensification and expansion of soil moisture drying in warm season over Eurasia under global warming. J. Geophys. Res. Atmos. 124(7), 3765-3782. https://doi.org/10.1029/2018JD029776.

Gu, X., Zhang, Q., Li, J., Singh, V.P., Liu, J., Sun, P., Cheng, C., 2019b. Attribution of global soil moisture drying to human activities: a quantitative viewpoint. Geophys. Res. Lett. 46, 2573-2582. https://doi.org/10.1029/2018GL080768.

Gudmundsson, L., Seneviratne, S.I., Zhang, X., 2017. Anthropogenic climate change detected in European renewable freshwater resources. Nat. Clim. Chang. 7(11), 813-816. https://doi.org/10.1038/NCLIMATE3416.

Harris, I., Osborn, T.J., Jones, P., Lister, D., 2020. Version 4 of the CRU TS monthly high-resolution gridded multivariate climate dataset. Sci. Data. 7(1), 1-18. https://doi.org/10.1038/s41597-020-0453-3.

Hannart, A. 2016. Integrated optimal fingerprinting: method description and illustration. J. Clim. 29(6), 1977-1998. https://doi.org/10.1175/JCLI-D-14-00124.1

Ingram, W., 2016. Extreme precipitation: Increases all round. Nat. Clim. Chang. 6(5), 443-444. https://doi.org/10.1038/nclimate2966.

Leng, G., Hall, J., 2019. Crop yield sensitivity of global major agricultural countries to droughts and the projected changes in the future. Sci. Total Environ. 654, 811-821. https://doi.org/10.1016/j.scitotenv.2018.10.434.

Li, M., Wu, P., Ma, Z., 2020. A comprehensive evaluation of soil moisture and soil temperature from third-generation atmospheric and land reanalysis data sets. Int. J. Climatol. 40(13), 5744-5766. https://doi.org/10.1002/joc.6549.

Liu, S., Chen, M., Zhuang, Q., 2016. Direct radiative effects of tropospheric aerosols on changes of global surface soil moisture. Clim. Change. 136(2), 175-187. https://doi.org/10.1007/s10584-016-1611-7.

Mahowald, N.M., 2011. Aerosol indirect effect on biogeochemical cycles and climate. Science, 334(6057), 794-796. https://doi.org/10.1126/science.1207374.

Martinez-Fernandez, J., Gonzalez-Zamora, A., Sanchez, N., Gumuzzio, A., 2015. A soil water based index as a suitable agricultural drought indicator. J. Hydrol. 522, 265-273. https://doi.org/10.1016/j.jhydrol.2014.12.051.

Martinez-Fernandez, J., Gonzalez-Zamora, A., Sanchez, N., Gumuzzio, A, Herrero-Jimenez, C.M., 2016. Satellite soil moisture for agricultural drought monitoring: assessment of the SMOS derived Soil Water Deficit Index. Remote Sens. Environ. 177, 277-286. https://doi.org/10.1016/j.rse.2016.02.064.

Minasny, B., Mcbratney, A.B., 2018. Limited effect of organic matter on soil available water capacity. Eur. J. Soil Sci. 69(1), 39-47. https://doi.org/10.1111/ejss.12475.

Mishra, A.K., Singh, V.P., 2010. A review of drought concepts. J. Hydrol. 391(1-2), 202-216. https://doi.org/10.1016/j.jhydrol.2010.07.012.

Mitchell, D., James, R., Forster, P.M., Betts, R.A., Shiogama, H., Allen, M., 2016.

Realizing the impacts of a 1.5 ºC warmer world. Nat. Clim. Chang. 6(8), 735-737. https://doi.org/10.1038/nclimate3055.

Nachtergaele, F.O., van Velthuizen, H., Verelst, L., Wiberg, D., Batjes, N.H., Dijkshoorn, J.A., van Engelen, V.W.P., Fischer, G., Jones, A., Montanarella, L., Petri, M., Prieler, S., Teixeira, E., Shi, X., 2012. Harmonized World Soil Database (version 1.2). Laxenburg, Austria: Food and Agriculture Organization of the UN, International Institute for Applied Systems Analysis, ISRIC - World Soil Information, Institute of Soil Science - Chinese Academy of Sciences, Joint Research Centre of the EC.

Naumann, G., Alfieri, L., Wyser, K., Mentaschi, L., Betts, R.A., Carrao, H., Spinoni, J., Vogt, J., Feyen, L., 2018. Global changes in drought conditions under different levels of warming. Geophys. Res. Lett. 45(7), 3285-3296. https://doi.org/10.1002/2017GL076521.

Ochsner, T.E., Cosh, M.H., Cuenca, R.H., Dorigo, W., Draper, C., Hagimoto, Y., Kerr, Y.H., Larson, K.M., Njoku, E.G., Small, E.E., Zreda, M.G., 2013. State of the art in large-scale soil moisture monitoring. Soil Sci. Soc. Am. J. 77(6), 1888-1919. https://doi.org/10.2136/sssaj2013.03.0093.

Othman, A. A., Obaid, A. K., Al-Manmi, D. A. M. A., Al-Maamar, A. F., Hasan, S. E., Liesenberg, V., ... & Al-Saady, Y. I. (2021). New insight on soil loss estimation in the northwestern region of the Zagros fold and thrust belt. ISPRS International Journal of Geo-Information, 10(2), 59.

Parajka, J., Naeimi, V., Blöschl, G., Komma, J., 2009. Matching ERS scatterometer based soil moisture patterns with simulations of a conceptual dual layer hydrologic model over Austria. Hydrol. Earth Syst. Sci. 13(2), 259-271. https://doi.org/10.5194/hess-13-259-2009.

Padron, R.S., Gudmundsson, L., Seneviratne, S.I., 2019. Observational constraints reduce likelihood of extreme changes in multidecadal land water availability. Geophys. Res. Lett. 46(2), 736-744. https://doi.org/10.1029/2018GL080521.

Palmer, W. C. (1965). Meteorological drought. Office of Climatology Research Paper 45, Weather Bureau, Washington, D.C., 58 pp.S

Parchami-Araghi, F., Mirlatifi, S.M., Dashtaki, S.G., Mahdian, M.H., 2013. Point estimation of soil water infiltration process using Artificial Neural Networks for some calcareous soils. J. Hydrol. 481, 35-47. https://doi.org/10.1016/j.jhydrol.2012.12.007.

Pradhan, P., Costa, L., Rybski, D., Lucht, W., Kropp, J.P., 2017. A systematic study of Sustainable Development Goal (SDG) interactions. Earth Future. 5(11), 1169–1179. https://doi.org/10.1002/2017EF000632.

Prudhomme, C., Giuntoli, I., Robinson, E.L., Clark, D.B., Arnell, N.W., Dankers, R., Fekete, B.M., Franssen, W., Gerten, D., Gosling, S.N., Hagemann, S., Hannah, D.M., Kim, H., Masaki, Y., Satoh, Y., Stacke, T., Wada, Y., Wisser, D., 2014. Hydrological droughts in the 21st century, hotspots and uncertainties from a global multimodel ensemble experiment. Proc. Natl. Acad. Sci. U. S. A. 111(9), 3262-3267. https://doi.org/10.1073/pnas.1222473110.

Ribes, A., Azais, J., Planton, S., 2009. Adaptation of the optimal fingerprint method for climate change detection using a well-conditioned covariance matrix estimate. Clim. Dyn. 33(5), 707-722. https://doi.org/10.1007/s00382-009-0561-4.

Ribes, A., Planton, S., Terray, L., 2013. Application of regularised optimal fingerprinting to attribution. Part I: method, properties and idealised analysis. Clim. Dyn. 41(11), 2817-2836. https://doi.org/10.1007/s00382-013-1735-7.

Rivas-Tabares, D., de Miguel, Á., Willaarts, B., & Tarquis, A. M. (2020). Self-organizing map of soil properties in the context of hydrological modeling. Applied mathematical modelling, 88, 175-189.

Rodell, M., Houser, P.R., Jambor, U., Gottschalck, J., Mitchell, K., Meng, C.J., Arsenault, K., Cosgrove, B., Radakovich, J., Bosilovich, M., Entin, J.K., Walker, J.P., Lohmann, D., Toll, D., 2004. The global land data assimilation system. Bull. Amer. Meteorol. Soc. 85(3), 381-394. https://doi.org/10.1175/BAMS-85-3-381.

Roux, P.C., Aalto, J., Luoto, M., 2013. Soil moisture's underestimated role in climate change impact modelling in low-energy systems. Glob. Change Biol. 19(10), 2965-2975. https://doi.org/ 10.1111/gcb.12286.

Samaniego, L., Thober, S., Kumar, R., 2018. Anthropogenic warming exacerbates European soil moisture droughts. Nat. Clim. Chang. 8, 421–426. https://doi.org/10.1038/s41558-018-0138-5.

Santos, W.J.R., Silva, B.M., Oliveira, G.C., Volpato, M.M.L., Lima, J.M., Curi, N., Marques, J.J., 2014. Soil moisture in the root zone and its relation to plant vigor assessed by remote sensing at management scale. Geoderma, 221, 91-95. https://doi.org/10.1016/j.geoderma.2014.01.006.

Seager, R., Ting, M., Held, I., Kushnir, Y., Lu, J., Vecchi, G., Huang, H., Harnik, N., Leetmaa, A., Lau, N., Li, C., Velez, J., Naik., N., 2007. Model projections of an imminent transition to a more arid climate in southwestern North America. Science, 316(5828), 1181-1184. https://doi.org/10.1126/science.1139601.

Sheffield, J., Wood, E.F., Roderick, M.L., 2012. Little change in global drought over the past 60 years. Nature. 491, 435–438. https://doi.org/10.1038/nature11575.

Shepherd, A., Martin, M., & Hastings, A. (2021). Uncertainty of modelled bioenergy with carbon capture and storage due to variability of input data. GCB Bioenergy, 13(4), 691-707.

Silatsa, F. B., Yemefack, M., Tabi, F. O., Heuvelink, G. B., & Leenaars, J. G. (2020). Assessing countrywide soil organic carbon stock using hybrid machine learning modelling and legacy soil data in Cameroon. Geoderma, 367, 114260.

Slangen, A.B., Church, J.A., Zhang, X., Monselesan, D., 2014. Detection and attribution of global mean thermosteric sea-level change. Geophys. Res. Lett. 41(16), 5951-5959. https://doi.org/10.1002/2014GL061356.

Suroso, Putudewi, A., & Ardiansyah. (2021). Impact of land use changes on the water availability in ciwulan watershed, west java. IOP Conference Series Earth and Environmental Science, 653(1), 012031.

Taylor, K.E., Stouffer, R.J., Meehl, G.A., 2012. An overview of CMIP5 and the experiment design. Bull. Amer. Meteorol. Soc. 93(4), 485–498. https://doi.org/10.1175/BAMS-D-11-00094.1.

Trenberth, K.E., Dai, A., Van Der Schrier, G., Jones, P.D., Barichivich, J., Briffa, K.R., Sheffield, J., 2014. Global warming and changes in drought. Nat. Clim. Chang. 4(1), 17–22. https://doi.org/10.1038/NCLIMATE2067.

Van der Schrier, G.V., Barichivich, J., Briffa, K.R., Jones, P.D., 2013. A scPDSI-based global data set of dry and wet spells for 1901-2009. J. Geophys. Res. Atmos. 118(10), 4025-4048. https://doi.org/10.1002/jgrd.50355.

Wanders, N., Bierkens, M.F., de Jong, S.M., de Roo, A., Karssenberg, D., 2014. The benefits of using remotely sensed soil moisture in parameter identification of large-scale hydrological models. Water Resour. Res. 50(8), 6874-6891. https://doi.org/10.1002/2013WR014639.

Wang, G., 2005. Agricultural drought in a future climate: Results from 15 global climate models participating in the IPCC 4th assessment. Clim. Dyn. 25, 739-753. https://doi.org/10.1007/s00382-005-0057-9.

Wells, N., Goddard, S., Hayes, M.J., 2004. A self-calibrating palmer drought severity index. J. Clim. 17(12), 2335-2351. https://doi.org/10.1175/1520-0442(2004)017<2335:ASPDSI>2.0.CO;2.

Wenjie, Z. H. U., Yang, G. A. O., & Cuiling, S. O. N. G. (2020). Dataset of the land use pattern optimization in Horqin Sandy Land. Data in brief, 33, 106335.

Wheeler, T.R., von Braun, J., 2013. Climate change impacts on global food security. Science, 341(6145), 508-513. https://doi.org/10.1126/science.1239402.

Yu, H., Zhang, Q., Xu, C.Y., Du, J., Sun, P., Hu, P., 2019. Modified Palmer Drought Severity Index: model improvement and application. Environ. Int. 130, 104951. https://doi.org/10.1016/j.envint.2019.104951.

Yuan, S., Quiring, S.M., 2017. Evaluation of soil moisture in CMIP5 simulations over the contiguous United States using in situ and satellite observations. Hydrol. Earth Syst. Sci. 21(4), 2203-2218. https://doi.org/10.5194/hess-21-2203-2017.

Yuan, X., Wang, L., Wu, P., Ji, P., Sheffield, J., Zhang, M., 2019. Anthropogenic shift towards higher risk of flash drought over China. Nat. Commun. 10, 4661. https://doi.org/10.1038/s41467-019-12692-7.

Zeng, J., Li, Z., Chen, Q., Bi, H., Qiu, J., Zou, P., 2015. Evaluation of remotely sensed and reanalysis soil moisture products over the Tibetan plateau using in-situ observations. Remote Sens. Environ. 163, 91–110. https://doi.org/10.1016/j.rse.2015.03.008.

Zhai, J., Huang, J., Su, B., Cao, L., Wang, Y., Jiang, T., Fischer, T., 2017. Intensity–area–duration analysis of droughts in China 1960–2013. Clim. Dyn. 48(1-2), 151-168. https://doi.org/10.1007/s00382-016-3066-y.

Zhang, L., Zhou, T., 2015. Drought over East Asia: a review. J. Clim. 28(8), 3375-3399. https://doi.org/10.1175/JCLI-D-14-00259.1.

Zhang, Q., Yu, H., Sun, P., Singh, V.P., Shi, P., 2019a. Multisource data based agricultural drought monitoring and agricultural loss in China. Glob. Planet. Change. 172, 298-306. https://doi.org/10.1016/j.gloplacha.2018.10.017.

Zhang, Q., Fan, K., Singh, V.P., Sun, P., Shi, P., 2018a. Evaluation of remotely sensed and reanalysis soil moisture against in-situ observations on the Himalayan-Tibetan Plateau. J. Geophys. Res. Atmos. 123, 7132-7148. https://doi.org/10.1029/2017JD027763.

Zhang, Q., Li, Q., Singh, V.P., Shi, P., Huang, Q., Sun, P., 2018b. Nonparametric integrated agrometeorological drought monitoring: model development and application. J. Geophys. Res. Atmos. 123, 73-88. https://doi.org/10.1002/2017JD027448.

Zhang, Q., Li, J., Singh, V.P., Xiao, M., 2013. Spatio-temporal relations between temperature and precipitation regimes: Implications for temperature-induced changes in the hydrological cycle. Glob. Planet. Change. 111, 57-76. https://doi.org/10.1016/j.gloplacha.2013.08.012.

Zhang, Q., Fan, K., Singh, V.P., Song, C., Xu, C., Sun, P., 2019b. Is Himalayan-Tibetan Plateau “drying”? Historical estimations and future trends of surface soil moisture. Sci. Total Environ. 658, 374-384. https://doi.org/10.1016/j.scitotenv.2018.12.209.

Zhang, X., Zwiers, F.W., Hegerl, G.C., Lambert, F.H., Gillett, N.P., Solomon, S., Stott, P.A., Nozawa, T., 2007. Detection of human influence on twentieth-century precipitation trends. Nature. 448(7152), 461-465. https://doi.org/10.1038/nature06025.

Zhu, Q., Luo, Y., Xu, Y. P., Tian, Y., Yang, T., 2019. Satellite soil moisture for agricultural drought monitoring: assessment of SMAP-derived Soil Water Deficit Index in Xiang River basin, China. Remote Sens. 11(3), 362. https://doi.org/10.3390/rs11030362.

Highlights

1. We evaluated soil moisture droughts with duration, magnitude and extremum in monsoon and non-monsoon regions;

2. We identified more evident impacts of anthropogenic forcing on soil moisture drought in monsoon region than in non-monsoon region;

3. We found larger impacts of anthropogenic forcing on drought magnitude, relative to drought duration and drought extremum.